NATIONAL AERONAUTICS AND SPACE ADMINISTRATION

Technical Report 32-1463

A Numerical Study of Cavity Radiometer Emissivities

C. L. Sydnor

JET PROPULSION LABORATORY
CALIFORNIA INSTITUTE OF TECHNOLOGY
PASADENA, CALIFORNIA

February 15, 1970

NATIONAL AERONAUTICS AND SPACE ADMINISTRATION

Technical Report 32-1463

A Numerical Study of Cavity Radiometer Emissivities

C. L. Sydnor

JET PROPULSION LABORATORY
CALIFORNIA INSTITUTE OF TECHNOLOGY
PASADENA, CALIFORNIA

February 15, 1970

Prepared Under Contract No. NAS 7-100
National Aeronautics and Space Administration

Preface

The work described in this report was performed by the Environmental Sciences Division of the Jet Propulsion Laboratory.

Acknowledgments

The author wishes to express his appreciation to C. M. Berdahl and R. E. Martin for support, to R. C. Willson and J. M. Kendall, Sr., for many helpful discussions, to B. A. Peavy of the National Bureau of Standards for a listing and explanation of his program, to D. L. Stierwalt of the Naval Weapons Center, Corona, California, for permission to reproduce some of his data on Parsons' black lacquer, and to W. L. Michalsky for reports coordination.

Contents

Tables

Contents (contd)

Figures

Abstract

Approximate and exact calculations of apparent emissivities were made for a variety of gray, uniform, isothermal, and Lambertian cavities. Some of these cavities are used in radiometers at the Jet Propulsion Laboratory. For a surface emissivity of 0.95, the cavity emissivity varied from 0.9820 for a simple cone of apex half-angle equal to 11.75 deg, to 0.9963 for a three-section cavity that was roughly semispherical in shape. An error analysis showed that the estimated error in the calculations was four parts in 100,000.

A perturbation method showed that in the cone cavity the surface was not actually isothermal but had a temperature variation of 0.5°C. The effect of this non-isothermality on the apparent cavity emissivity was to change it from 0.9820 to 0.9809, for a surface emissivity of 0.95. Corresponding figures for one of the three-section cavities studied were 0.13°C for the temperature variation and a change from 0.9909 to 0.9923 for the cavity emissivity.

When the surface emissivity was assumed to have a particular dependence on wavelength, the cavity emissivity was shown to vary from 0.9676 at 250°K to 0.9698 at 500°K as a result of the shift in the peak of the blackbody function. Corresponding figures for a three-section cavity were from 0.9848 at 250°K to 0.9858 at 500°K. For comparison, a flat plate with the same assumed wavelength dependence of emissivity was shown to vary from an effective emissivity of 0.9127 at 250°K to 0.9183 at 500°K.

A Numerical Study of Cavity Radiometer Emissivities

I. Introduction

Extensive experimental and theoretical work has been done at the Jet Propulsion Laboratory (JPL) on cavity radiometers during the past few years (Refs. 1–6). Part of this work has consisted of performing calculations that better establish the emissive properties of cavities. This report presents some of those calculations.

It is well established that the apparent emissivity of a cavity aperture is greater than the emissivity of the inner surface of the cavity. Planck, for example, in Ref. 7, discusses the fact that an isothermal cavity with a small aperture appears essentially black. Various authors have made calculations of the enhancement in emissivity caused by the cavity. Approximate calculations have been made, for example, in Refs. 8 and 9 and exact analytical or numerical calculations in Refs. 10–13. In this report both approximate and exact methods are used where appropriate.

For the purposes of this report the calculations were made of the apparent emissivity, although the absorptivity could have been calculated instead. An isothermal cavity at temperature T will radiate with an emissivity ϵ_a, and if this cavity receives hemispherical black body radiation at its aperture from surroundings at the same temperature T, the apparent absorptivity α_a will be equal to ϵ_a.

For many of the applications of this report, therefore, we can take the apparent absorptivity to be equal to the apparent emissivity.

Under some circumstances, however, $\alpha_a \neq \epsilon_a$; for example, when the temperature T_1 of incoming blackbody radiation is much different from the temperature T_2 of the cavity. Then the ϵ_a for T_2 may be different from ϵ_a for T_1, as shown in Section VI, and thus $\alpha_a \neq \epsilon_a$.

II. Approximate Determination of the Emissivity of Isothermal Cavities

A. Methods

For purposes of design, it was desired to find the approximate apparent emissivity of cavities having a variety of configurations. The assumptions adopted for this section are that the cavities are:

(1) Isothermal.

(2) Gray (no wavelength dependence of properties).

(3) Uniform.

(4) Lambertian (emit, reflect, and absorb diffusely).

It was assumed initially and later verified that the approximate method of Treuenfels, Ref. 8, was adequate for this purpose. This method assumes that the fractions of the exitance emerging from a point x after one reflection, two reflections, etc. decrease in a constant ratio β. For full details see Treuenfels' paper. The results to be used here are that if $f = 1 - \beta$, then we have the apparent emissivity ϵ_a is given by

$$\epsilon_a = \frac{\epsilon}{\epsilon + f(1-\epsilon)} \tag{1}$$

where

$$f = \frac{\int_x (F_{x-o})^2 \, da\,(x)}{\int_x F_{x-o} \, da\,(x)} \tag{2}$$

and x is a running variable in the cavity (Fig. 1). Note that x may run from the apex to the aperture or vice-versa, whichever is more convenient. F_{x-o} is the view factor from x to the aperture; $da\,(x)$ is the element of area in the cavity. A full discussion of the meaning of view factors or angle factors is given in Ref. 14. Briefly, the view factor F_{1-2} is the fraction of blackbody power leaving surface 1 that arrives at surface 2.

The cavities studied are shown in Figs. 2–6. The appropriate view factors (F_{1o}, F_{2o}, and F_{3o}) are given in the appendix. These were obtained by the method of view factor or angle factor algebra discussed, for example, in Ref. 14. The same view factors are used for cavities II–V as are used for cavity I, if the dimensions are defined appropriately. The variables used in the view factors are defined in the appendix and in Fig. 2.

After the view factors were obtained a computer program was written in FORTRAN II for the IBM 1620. Its purpose was to calculate the flatness f and the apparent cavity emissivity ϵ_a for a range of surface emissivities ϵ. The dimensions of the cavity are inputs in the program,

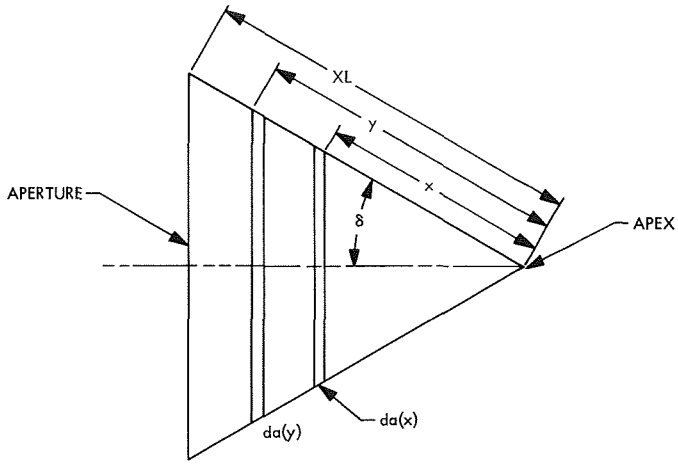

Fig. 1. Cavity geometry

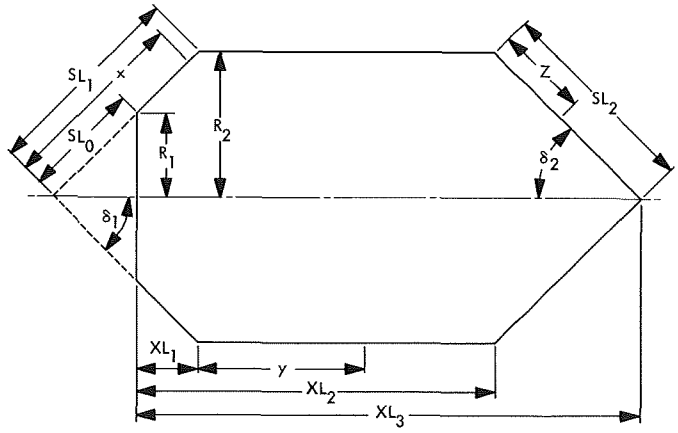

Fig. 2. Cavity I

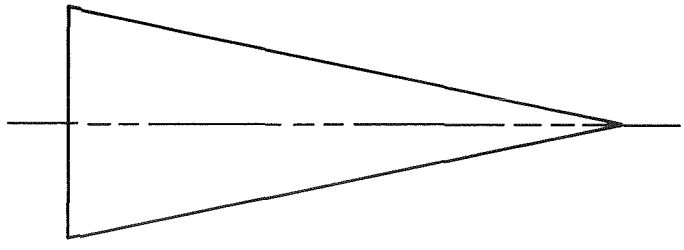

Fig. 3. Cavity II

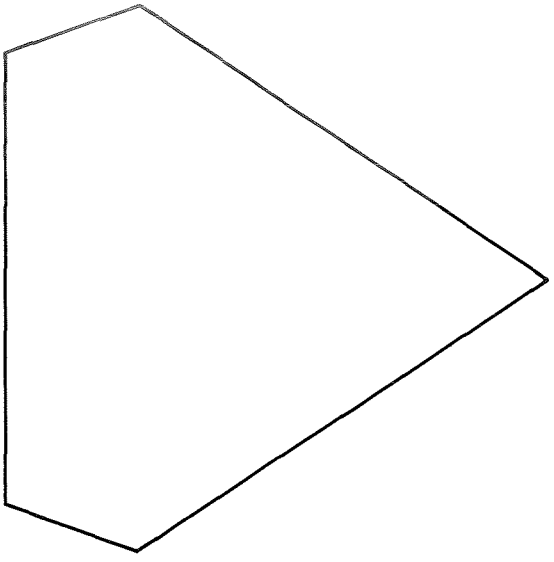

Fig. 4. Cavity III

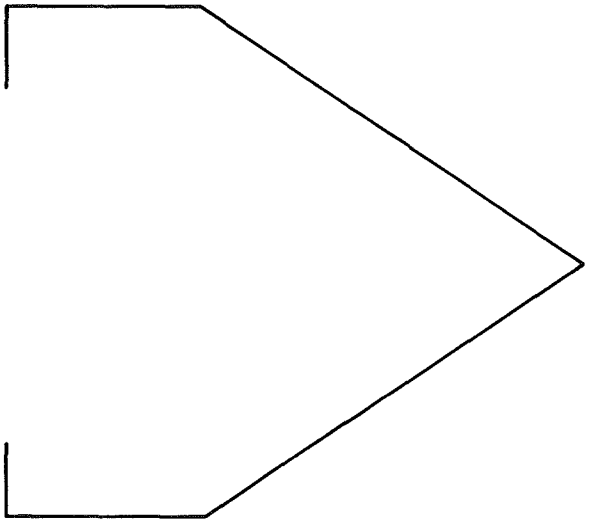

Fig. 5. Cavity IV

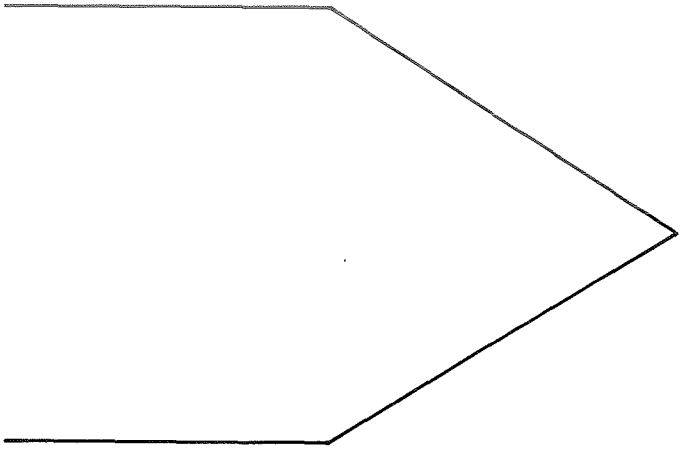

Fig. 6. Cavity V

therefore many different cavities may be studied providing they conform to any of the basic shapes of cavities I–V. The integration was performed using Simpson's rule, with 100 intervals of integration.

B. Results

The results of the approximate calculations are presented in Table 1 and Table 2. Table 1 shows the dimensions of the various cavities studied and also the computed value of f for each of these cavities. There are five cavities having the general configuration of the cavity shown in Fig. 2, but with slightly different dimensions. These are identified in Table 1 as cavities Ia–Ie. Table 2 gives the apparent emissivity ϵ_a of each of these cavities over a range of surface emissivities ϵ. These values of ϵ_a were computed using Eq. (1). The results are given to only three decimal places for reasons to be explained in Section IV. Cavities Ia, Ie, and II were subjected to further study. The results of this further study are presented in succeeding portions of this report.

Table 1. Dimensions of cavities used in calculations

Cavity	XL_1, cm	XL_2, cm	XL_3, cm	SL_0, cm	SL_1, cm	SL_2, cm	R_1, cm	R_2, cm	δ_1, deg	δ_2, deg	f
Ia	0.6	1.8	3.3	0.83	1.45	1.9	0.54	0.95	42.0	30.0	0.06823
Ib	0.219	1.437	2.312	0.875	1.219	1.219	0.58	0.844	45.0	45.0	0.11149
Ic	0.6	1.825	3.15	1.825	2.45	1.5	0.625	0.85	19.5	34.0	0.13342
Id	0.6	1.3	2.625	1.825	2.45	1.5	0.625	0.85	19.5	34.0	0.14248
Ie	0.475	1.269	2.142	1.943	2.44	1.129	0.568	0.714	17.021	39.293	0.15900
II	—	—	—	—	—	2.77	—	0.576	—	11.75	0.34502
III	0.6	0.6	1.93	1.825	2.45	1.5	0.625	0.85	19.5	34.0	0.18634
IV	0.0	0.7	2.03	—	—	1.5	0.625	0.85	—	34.0	0.16267
V	0.0	1.225	2.55	—	—	1.5	—	0.85	—	34.0	0.26555

Table 2. Approximate cavity emissivity ϵ_a for cavities used in calculations

Surface emissivity, ϵ	Cavity, ϵ_a								
	Ia	Ib	Ic	Id	Ie	II	III	IV	V
0.85	0.988	0.981	0.977	0.975	0.973	0.943	0.968	0.972	0.955
0.86	0.989	0.982	0.979	0.977	0.975	0.947	0.971	0.974	0.959
0.87	0.990	0.984	0.980	0.979	0.977	0.951	0.973	0.976	0.962
0.88	0.991	0.985	0.982	0.981	0.979	0.955	0.975	0.978	0.965
0.89	0.992	0.986	0.984	0.983	0.981	0.959	0.977	0.980	0.968
0.90	0.992	0.988	0.985	0.984	0.983	0.963	0.980	0.982	0.971
0.91	0.993	0.989	0.987	0.986	0.985	0.967	0.982	0.984	0.974
0.92	0.994	0.990	0.989	0.988	0.986	0.971	0.984	0.986	0.977
0.93	0.995	0.992	0.990	0.989	0.988	0.975	0.986	0.988	0.980
0.94	0.996	0.993	0.992	0.991	0.990	0.978	0.988	0.990	0.983
0.95	0.996	0.994	0.993	0.993	0.992	0.982	0.990	0.992	0.986
0.96	0.997	0.995	0.994	0.994	0.993	0.986	0.992	0.993	0.989
0.97	0.998	0.997	0.996	0.996	0.995	0.989	0.994	0.995	0.992
0.98	0.999	0.998	0.997	0.997	0.997	0.993	0.996	0.997	0.995
0.99	0.999	0.999	0.999	0.999	0.998	0.997	0.998	0.998	0.997
1.00	1.000	1.000	1.000	1.000	1.000	1.000	1.000	1.000	1.000

III. Exact Numerical Calculations of the Emissivity of Isothermal Cavities

A. Solution of the Integral Equation for Cavity Emissivity by the Method of Successive Approximations, Using Direct Iteration

In this section it is assumed again that the cavities to be discussed are:

(1) Isothermal.

(2) Gray.

(3) Uniform.

(4) Lambertian.

Under these conditions, the apparent emissivity $\epsilon(x)$ at a point x on the inner surface of the cavity is given exactly by the integral equation.

$$\epsilon(x) = \epsilon + \rho \int_y \epsilon(y)\, K(x,y)\, dy \tag{3}$$

Here ϵ is again the surface emissivity, ρ is the reflectivity, and $K(x,y)\,dy = dF_{x-y}$ is the view factor from area element $da(x)$ to area element $da(y)$ (see Fig. 1). The derivation of this equation is given several places in the literature and will not be repeated here. The clearest derivation seems to be that given in Ref. 10. According to Ref. 14, this equation has been solved analytically for only two cavity configurations, the spherical cavity and the cylindrical arc cavity (Ref. 12 and Ref. 13). For most cavities the equation must be solved numerically. A common approach is to apply numerically the method of successive approximations. A set of values $\epsilon(y)$ is assumed at a finite number of values of y and the integral

$$\int_y \epsilon(y)\, K(x,y)\, dy \tag{4}$$

is evaluated numerically for each x and upon substitution in Eq. (3), a set of values of $\epsilon(x)$ is obtained. This set is used as a second guess and is itself substituted in the integral, producing a new set of $\epsilon(x)$ on the left side of Eq. (3). This process is continued until convergence is achieved. The usual criterion for convergence is that successive sets of values of $\epsilon(x)$ must differ by a negligible amount.

Once the set of values $\epsilon(x)$ has been obtained, it is desired to find ϵ_a, the apparent emissivity of the cavity. One way to do this is as follows.

First, consider the definition of ϵ_a.

$$\epsilon_a = \frac{Q}{Q_b} \tag{5}$$

where Q is the radiant flux passing out the aperture and Q_b is the blackbody flux that would be emitted from a surface of area A stretched over the aperture. Then

$$Q_b = \sigma T^4 A \tag{6}$$

The total radiant flux from a zone of area $da(x)$ is $\epsilon(x)\,\sigma T^4\, da(x)$. The fraction of this flux which reaches the aperture is F_{x-o}, where F_{x-o} is the view factor from x to the aperture or opening. The flux reaching the aperture

from $da(x)$ is then $\epsilon(x)\,\sigma T^4\,da(x)\,F_{x-o}$. Therefore, the total flux reaching the aperture is

$$Q = \int_x \epsilon(x)\,\sigma T^4\,F_{x-o}\,da(x) \tag{7}$$

and

$$\epsilon_a = \frac{\int_x \epsilon(x)\,\sigma T^4\,F_{x-o}\,da(x)}{\sigma T^4 A} \tag{8}$$

$$\epsilon_a = \frac{\int_x \epsilon(x)\,F_{x-o}\,da(x)}{A} \tag{9}$$

The integral Equation (3) was solved by the direct iteration process just discussed for three of the cavities (Ia, Ie, and II) given in Table 1. The necessary view factors are given in the appendix. For cavities Ia and II, a surface emissivity of 0.95 was used, but for cavity Ie a surface emissivity of 0.945 was used. The results of these calculations are summarized in Table 3, where ϵ_a has been computed from Eq. (9).

It should be emphasized here that "exact" means the result of solving the integral Eq. (3) numerically, rather than using the approximate approach developed by Treuenfels and used in Section I, and does not mean using an analytical solution.

A question arising when these calculations are performed is the one of accuracy. This question is discussed in Section IV, but the results of that section are taken into cognizance in the retained significant figures given in this section.

Table 3. Exact cavity emissivity for several cavities

Cavity	Surface emissivity, ϵ	Cavity emissivity, ϵ_a
Ia (three-section cavity)	0.95	0.9963
Ie (three-section cavity)	0.945	0.9909
II (cone)	0.95	0.9820

B. Derivation of Series Representation of Solution of Integral Equation

After most of the calculations discussed in this report were performed, a better method than the direct iteration method was found to solve the integral Eq. (3). This method has been presented in Ref. 6. Most of the material from this reference is repeated in this report in a somewhat different form and is reproduced by permission of the Journal of the Optical Society of America. Instead of performing the successive approximations by direct iteration, as done previously, an equivalent series is developed.

To develop the series, let us examine the iterative method more closely. It can be shown (Ref. 15) that if the series solution for the integral Eq. (3) obtained by successive approximations converges to a solution, then this solution does not depend on the first guess. For the present purposes, however, it is desirable to use as a first guess simply the surface emissivity ϵ. We obtain from the first iteration, $\epsilon_1(x)$:

$$\epsilon_1(x) = \epsilon + \rho\epsilon \int K(x, y)\,dy \tag{10}$$

For the second iteration we have

$$\epsilon_2(z) = \epsilon + \rho\epsilon \int K(z, x)\,dx + \rho^2\epsilon \int [K(x, y)\,dy]\,[K(z, x)\,dx] \tag{11}$$

Continuing this process we arrive at the formula

$$\epsilon(x) = \epsilon[1 + \rho\phi_1(x) + \rho^2\phi_2(x) + \cdots + \rho^{n-1}\phi_{n-1}(x) + \cdots] \tag{12}$$

where

$$\phi_1(x) = \int K(x, y)\,dy \tag{13}$$

and

$$\phi_n(x) = \int K(x, y)\,\phi_{n-1}(y)\,dy\,, \qquad n = 2, 3, \cdots \tag{14}$$

The series, Eq. (12), is called the Neumann series for Eq. (3) and represents the solution to Eq. (3) if it converges (Ref. 16). One way to prove convergence is to use a physical argument. Multiply each term of the series by σT^4. This does not affect convergence. Now the terms of the series

$$R = \epsilon\sigma T^4 + \rho\epsilon\sigma T^4\,\phi_1(x) + \cdots + \rho^{n-1}\,\epsilon\sigma T^4\,\phi_{n-1}(x) + \cdots \tag{15}$$

have the following meaning. The first term is the emitted exitance at x. The second term represents that portion of the exitance at x which has arrived at x after being emitted in the rest of cavity and is then reflected at x. The third

and succeeding terms represent reflected exitance at x that has undergone one previous reflection, two previous reflections, etc. Therefore, the series must represent the total exitance at x and therefore converges to $\epsilon(x)\sigma T^4$. Thus the original series, Eq. (12), also converges and represents the solution to Eq. (3).

The series representation, Eq. (12), has several important advantages not apparent when the solution is obtained numerically by direct iteration, although, of course, the methods are equivalent since the series is obtained by means of iteration.

(1) An error bound ρ^{N+1} can be obtained, as discussed in Section IV.

(2) The result of N iterations is the algebraic form

$$\epsilon(x) \simeq \epsilon[1 + \rho\phi_1(x) + \rho^2\phi_2(x) + \cdots + \rho^N\phi_N(x)] \tag{16}$$

Once the ϕ_i terms are obtained numerically by iteration, using Eqs. (13) and (14), the set $\epsilon(x)$ and therefore ϵ_a can be calculated simply by evaluating the form (16) for each ϵ and ρ, without having to do the iteration over again for each ϵ and ρ. This is a considerable saving in computer time.

Although this method was developed after most of the desired calculations had been made, a program was written to try out the method with the cone, cavity II. The resulting ϵ_a for ϵ in the range 0.84 to 1.00 is shown in Table 4.

Table 4. Exact cavity emissivity ϵ_a for cone, cavity II, for surface emissivity ϵ in range 0.84 to 1.00

Surface emissivity, ϵ	Cavity emissivity, ϵ_a
0.84	0.939
0.85	0.943
0.86	0.947
0.87	0.9512
0.88	0.9552
0.89	0.9592
0.90	0.9631
0.91	0.9670
0.92	0.9708
0.93	0.9746
0.94	0.9783
0.95	0.9820
0.96	0.9857
0.97	0.9893
0.98	0.9929
0.99	0.9965
1.00	1.0000

IV. Error Analysis of Emissivity Calculations

A. Errors to be Discussed

If the results of emissivity calculations are to be applied to actual radiometers, the accuracy of the calculations is of interest. Errors can arise from two sources:

(1) Use of incorrect or incomplete assumptions about the properties and behavior of the cavities.

(2) Use of numerical methods.

The errors arising from the first source are by far the most difficult to treat. An attempt to estimate the effects of some of these errors is made in Sections V and VI, but the concern here is primarily with estimating the accuracy of the numerical calculations, and thus estimating the error in the numerical results used in Sections II and III, under the assumptions used there.

B. Errors in ϵ_a from Solution of Integral Equation

Errors in the values of ϵ_a calculated from the solution of the integral Eq. (3) and the use of Eq. (9) are of several types:

(1) Errors due to ending the iteration after a finite number of steps (truncation error).

(2) Error due to use of a finite number of integration steps (integration errors).

(3) Errors due to using finite arithmetic (chopping errors).

Irregularities in the functions occurring in the calculations cause particular difficulties in the evaluation of types (2) and (3) errors. Truncation errors are easy to treat, however, and a completely rigorous bound can be given for these errors (Ref. 6).

Suppose for now that the integrations indicated in Eqs. (13) and (14) for the evaluation of the ϕ_i terms can be performed as accurately as desired. Then the error of interest arises from using only a finite number of terms of the series, Eq. (12).

Let us rewrite the series

$$\epsilon(x) = \epsilon_N(x) + E(x) \tag{17}$$

where

$$\epsilon_N(x) = \epsilon[1 + \rho\phi_1(x) + \cdots + \rho^N\phi_N(x)] \tag{18}$$

and

$$E(x) = \epsilon\rho^{N+1}\left[\phi_{N+1}(x) + \cdots + \rho^{n-1}\phi_{N+n}(x) + \cdots\right] \tag{19}$$

The term $\epsilon_N(x)$ is the value used for $\epsilon(x)$ as the result of N iterations, that is, as the result of using $N+1$ terms of the series, Eq. (12), and $E(x)$ is the error in $\epsilon(x)$ resulting from dropping the remaining terms. Note that $E(x)$ is a series of positive terms, so there is some doubt about the accuracy of $\epsilon_N(x)$ as an estimate of $\epsilon(x)$. We can see that the requirement that differences between successive terms become small is not completely adequate justification for stopping the iteration, since an infinite sum of even very small terms may add to any desired number, even though we can see that Eq. (19) converges, since Eq. (12) converges.

To establish a bound on $E(x)$, let us first suppose, without loss of generality, that x ranges from 0 to 1. This is simply a convenience. Now we can show by induction on n that for all x in $(0, 1)$ and for all n,

$$O \leqq \phi_n(x) \leqq 1 \tag{20}$$

First,

$$O \leqq \phi_1(x) = \int_o^1 K(x,y)\,dy \leqq 1 \tag{21}$$

follows from the identity

$$\int_o^1 K(x,y)\,dy + F_{x\text{-}o} = 1 \tag{22}$$

where as before $F_{x\text{-}o}$ is the view factor from x to the aperture. This identity expresses the fact that the fractions of exitance from a surface must sum to 1. We have used also the fact that since $F_{x\text{-}o}$ represents a fraction of exitance,

$$O \leqq F_{x\text{-}o} \leqq 1 \tag{23}$$

Next, by the hypothesis $O \leqq \phi_n(y) \leqq 1$, and since $K(x,y) \geqq O$, as a result of its definition, we have $O \leqq K(x,y)\,\phi_n(y) \leqq K(x,y)$ and so

$$\begin{aligned} O \leqq \phi_{n+1}(x) &= \int K(x,y)\,\phi_n(y)\,dy \\ &\leqq \int K(x,y)\,dy \leqq 1 \end{aligned} \tag{24}$$

by the comparison test for integrals.

Therefore

$$\rho^n \geqq \rho^n\phi_i(x) \tag{25}$$

for any i and n, so

$$T = 1 + \rho + \rho^2 + \cdots + \rho^{n+1} + \cdots \tag{26}$$

dominates the series

$$S = \phi_{N+1}(x) + \cdots + \rho^{n-1}\phi_{N+n}(x) + \cdots \tag{27}$$

Thus $E(x) = \epsilon S$ converges, which we already knew, but furthermore since

$$S \leqq T = \frac{1}{1-\rho}, \qquad E(x) \leqq \frac{\epsilon\rho^{N+1}}{1-\rho}.$$

Using $\epsilon = 1 - \rho$ we have

$$E(x) \leqq \rho^{N+1} \tag{28}$$

Therefore the truncation error in each $\epsilon_N(x)$ is less than or equal to ρ^{N+1}. Now we want to find an error bound on ϵ_a resulting from the bound on the error in the calculated $\epsilon(x)$. To do this, recall Eq. (9):

$$\epsilon_a = \frac{1}{A}\int_x \epsilon(x)\,F_{x\text{-}o}\,da(x) \tag{29}$$

From Eqs. (17) and (28) we have

$$\epsilon_a = \frac{1}{A}\int_x \epsilon_N(x)\,F_{x\text{-}o}\,da(x) + \frac{1}{A}\int_x E(x)\,F_{x\text{-}o}\,da(x) \tag{30}$$

or

$$\epsilon_a(\text{true}) = \epsilon_a(\text{numerical}) + E \tag{31}$$

where

$$E = \frac{1}{A}\int E(x)\,F_{x\text{-}o}\,da(x) \leqq \frac{1}{A}\int \rho^{N+1}\,F_{x\text{-}o}\,da(x) \tag{32}$$

since

$$E(x) \leqq \rho^{N+1} \tag{33}$$

If we suppose for the moment that the surface is black, then $\epsilon(x) = \epsilon_a = 1$, and from Eq. (29) we have

$$1 = \frac{1}{A}\int_x F_{x\text{-}o}\,da(x) \tag{34}$$

This identity is an expression of the fact that terms of the form (area x projected angle), which are discussed in

Ref. 17 and which have been called "throughput," for example, in Ref. 18, must be constant for any surface bounded by the edge of the aperture. This is to say, the throughput for the inner surface of the cavity, $\int F_{x-o}\, da\,(x)$, must equal the throughput for the aperture, A (area) $\times$ 1 hemisphere (projected solid angle).

Now applying Eq. (34) to Eq. (33) we have

$$E \leqq \rho^{N+1} \tag{35}$$

Thus we have the result that the truncation error in ϵ_a is less than ρ^{N+1}.

This error bound is rigorous, but the treatment of integration errors is not. There is somewhat more than the usual problem with performing the integrations necessary to evaluate the terms $\phi_i\,(x)$. This difficulty is caused by the fact that for both cavities I and II, the kernel of the integral equation $K(x, y)$, has a slope discontinuity at $x = y$. This is shown, for example, in Fig. 7, where $K_{22}\,(x, y)\,dy = dF_{22}\,(x, y)$ is given in the appendix. For this plot, y ranges over 31 equispaced values y_i ranging from 0 to 0.794 and $x = y_{10} = 0.2382$.

A possible problem with this slope discontinuity is that errors may occur if Simpson's rule is used. To see this, recall that Simpson's rule requires the use of an odd number of points N in the range of integration, including the end points, defining an even number of intervals $M = N - 1$. Simpson's rule fits a parabola through successive sets of three points. Now in $K(x, y)$, suppose that integration takes place with respect to y and that x is a parameter. If x is coincident with one of the odd points in the mesh, Fig. 8 shows the curve fit, but if x is an even point, Fig. 9 is appropriate. The fit in Fig. 9 is not reasonable.

This problem has been treated several different ways in the literature. For example, Sparrow and Jonsson (Ref. 10) performed the integration separately on each side of the slope discontinuity. Peavy (Ref. 11) used a substitution technique which made the integrand equal to 0 at the slope discontinuity and close to 0 near it.

The method adopted for the calculations reported here was to use Simpson's rule when x was an odd point, but when x was an even point, Simpson's rule was used for all but the point x and the two points on each side of it. For these points the trapezoid rule was used, as shown in Fig. 10.

This method of integration was applied to cavities Ia, Ie, and II, using direct iteration, with the results shown

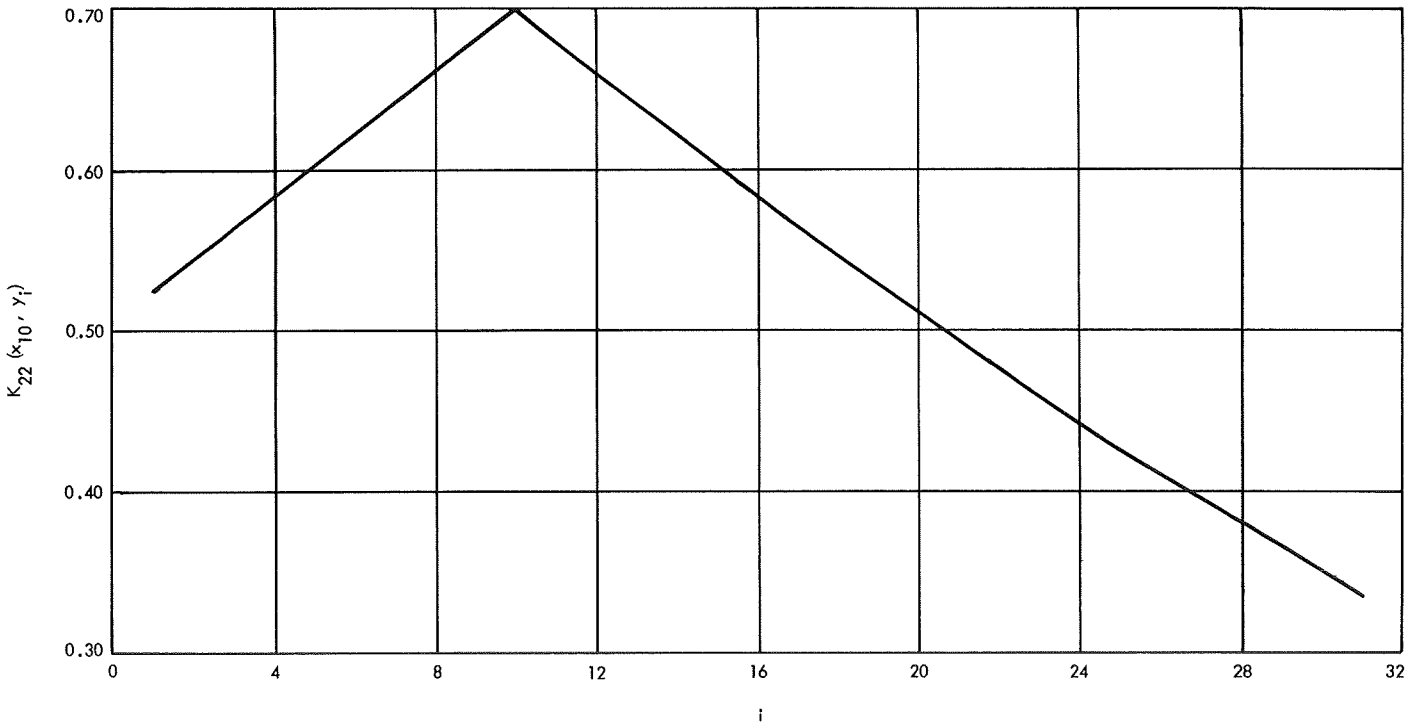

Fig. 7. Slope discontinuity as shown by plot of cavity Ie view factor

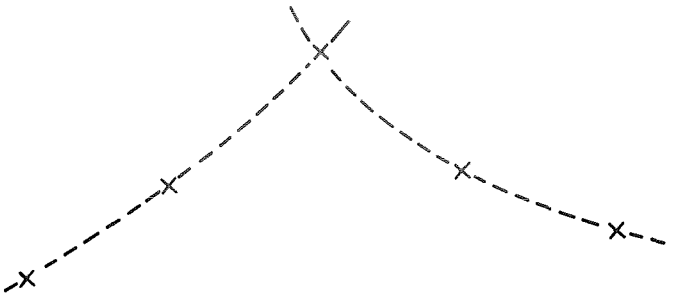

Fig. 8. Parabolic curve fit, odd point

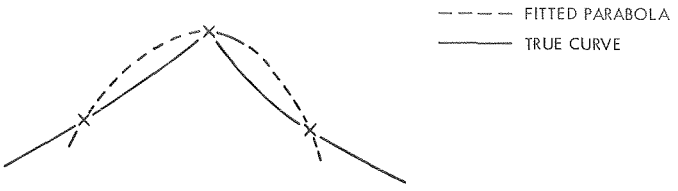

Fig. 9. Parabolic curve fit, even point

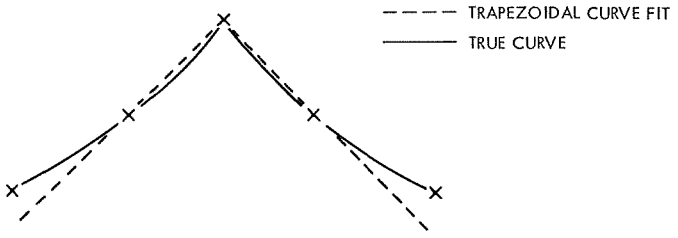

Fig. 10. Trapezoidal curve fit, even point

in Table 3. For the cone, cavity II, 100 intervals of integration were used, and for cavities Ia and Ie, 93 intervals (31 in each section). Essentially the same method was applied to non-isothermal cavities, discussed in Section V.

The accuracy of these calculations is believed to be comparable to that of the results previously reported in the literature of numerical solutions of the integral equation. Indeed, when the method of Peavy (Ref. 11) was applied to cavity II, using 100 intervals of integration and double precision on the IBM 7094, the result obtained was

$$\epsilon_a = 0.98203316 \tag{36}$$

whereas the result of the method given here was

$$\epsilon_a = 0.98201881 \tag{37}$$

This was obtained using 100 intervals of integration and a floating point precision (fpp) equal to 12 digits.

These answers are the same within two parts per 100,000, a reasonable agreement. However, the results of these calculations showed somewhat erratic behavior of $\epsilon(x)$ for positions near the apex. Table 5 presents $\epsilon(x)$ vs station number, with the stations numbered from apex to aperture. Note that there are some values of $\epsilon(x)$ near the apex which are even greater than 1.

These irregular values of $\epsilon(x)$ near the apex arise from two sources:

(1) The effect of finite intervals on the integration becomes more important for intervals near the apex.

(2) $K(x, y)$ for the cone is given in the appendix, where the dimensions are as in Fig. 1. Study of this function shows that there is a singularity at $x = 0$. When using finite arithmetic the effect of this singularity is felt even for small but nonzero values of x, that is, chopping errors are important.

These effects have been mentioned already as possible general sources of error; we see now that they are especially important near the apex.

To alleviate this problem we can:

(1) Substitute an algebraic formula for at least some of the integrals.

(2) Decrease the interval size.

(3) Increase the precision of the numbers used in the calculation.

Consider first the substitution of an algebraic expression for the integrals. This is essentially what Peavy has done in Ref. 11. He has developed an algebraic formula for the integral appearing in the first iteration. Since the errors mentioned are errors in $K(x, y)$ and $\int K(x, y)\, dy$, it can be seen that substituting an algebraic expression for the first integration should be effective in reducing error, since an algebraic expression which has no singularities should be easier to evaluate accurately than either $K(x, y)$ or $\int K(x, y)\, dy$.

Since Peavy's method gave essentially the same ϵ_a (and incidentally still produced one $\epsilon(x) > 1$ near the apex) it was apparent that either the result obtained here was accurate or that both this result and the result from Peavy's method were inaccurate. To try to get a cross check on both methods a different approach was used. The basis of this was the algebraic form used in Eq. (16). Here we use four iterations. With $\epsilon = 0.95$, $\rho = 0.05$ and $\rho^5 = 3 \times 10^{-7}$, which is negligible. Indeed, this number of iterations was used throughout this report.

Table 5. Emissivity of cone by direct iteration ($M = 100$, fpp = 12, $\epsilon = 0.95$)

Station No.	ϵ (x)	Station No.	ϵ (x)
1	0.99955572	52	0.99704454
2	0.12760062	53	0.99690493
3	0.94642189	54	0.99675791
4	1.0158988	55	0.99660251
5	1.0095168	56	0.99643873
6	1.0013271	57	0.99626563
7	1.0037116	58	0.99608308
8	0.99992495	59	0.99589016
9	1.0017504	60	0.99568663
10	0.99959561	61	0.99547115
11	1.0008548	62	0.99524459
12	0.99946321	63	0.99500479
13	1.0003536	64	0.99475172
14	0.99938218	65	0.99448441
15	1.0000325	66	0.99420234
16	0.99931666	67	0.99390450
17	0.99969051	68	0.99359030
18	0.99925518	69	0.99325873
19	0.99921505	70	0.99290910
20	0.99919425	71	0.99254041
21	0.99915704	72	0.99215192
22	0.99913157	73	0.99174263
23	0.99909450	74	0.99131177
24	0.99906482	75	0.99085834
25	0.99902647	76	0.99038159
26	0.99899271	77	0.98988057
27	0.99895213	78	0.98935455
28	0.99891423	79	0.98880266
29	0.99887067	80	0.98822422
30	0.99882843	81	0.98761848
31	0.99878125	82	0.98698488
32	0.99873435	83	0.98632279
33	0.99868293	84	0.98563181
34	0.99863097	85	0.98491149
35	0.99857469	86	0.98416162
36	0.99851716	87	0.98338197
37	0.99845536	88	0.98257252
38	0.99839168	89	0.98173331
39	0.99832364	90	0.98086456
40	0.99825312	91	0.97996655
41	0.99817807	92	0.97903976
42	0.99809992	93	0.97808473
43	0.99801697	94	0.97710220
44	0.99793033	95	0.97609296
45	0.99783851	96	0.97505798
46	0.99774236	97	0.97399826
47	0.99764058	98	0.97291500
48	0.99753379	99	0.97180938
49	0.99742082	100	0.97068276
50	0.99730212	101	0.96953647
51	0.99717659		

Recall Eq. (13) and Eq. (22):

$$\phi_1(x) = \int_o^1 K(x, y)\, dy \tag{38}$$

and

$$\int_o^1 K(x, y)\, dy + F_{x-o} = 1 \tag{39}$$

From these we obtain

$$\phi_1(x) = 1 - F_{x-o} \tag{40}$$

F_{x-o} is a well behaved function and is given in the appendix. It is also plotted versus x in Fig. 11. The only irregularity is at $x = 1$ and the value there can be obtained by quadratic extrapolation. Alternatively, we can construct F_{x-o} for finite zones in the cavity by the method of angle-factor algebra mentioned earlier.

Thus, by use of Eq. (40), we avoid one use of $K(x, y)$, with its attendant chopping errors, and also one integration, with its integration errors, and instead evaluate the straightforward form F_{x-o}.

It is worthwhile, examining F_{x-o} a little closer, to see if F_{x-o} really gives more accurate values of $\phi_1(x)$ than Eq. (38).

From Eq. (34)

$$I_1 = \frac{1}{A}\int F_{x-o}\, da(x) = 1 \tag{41}$$

If we actually perform this integration numerically, using $M = 100$ intervals of integration and fpp = 12, we obtain

$$I_1 = 1.0000007680 \tag{42}$$

From Eq. (39) we have

$$F_{x-o} = 1 - \int_o^1 K(x, y)\, dy \tag{43}$$

so

$$I_2 = \frac{1}{A}\int_x \left[1 - \int K(x, y)\, dy\right] da(x) = 1 \tag{44}$$

If we evaluate I_2 numerically, recognizing that $\int da(x) =$ surface area, we obtain

$$I_2 = 0.98940017672 \tag{45}$$

We can see that in the sense of some sort of mean-over-area that F_{x-o} can be evaluated more accurately than $\int K(x, y)\, dy$.

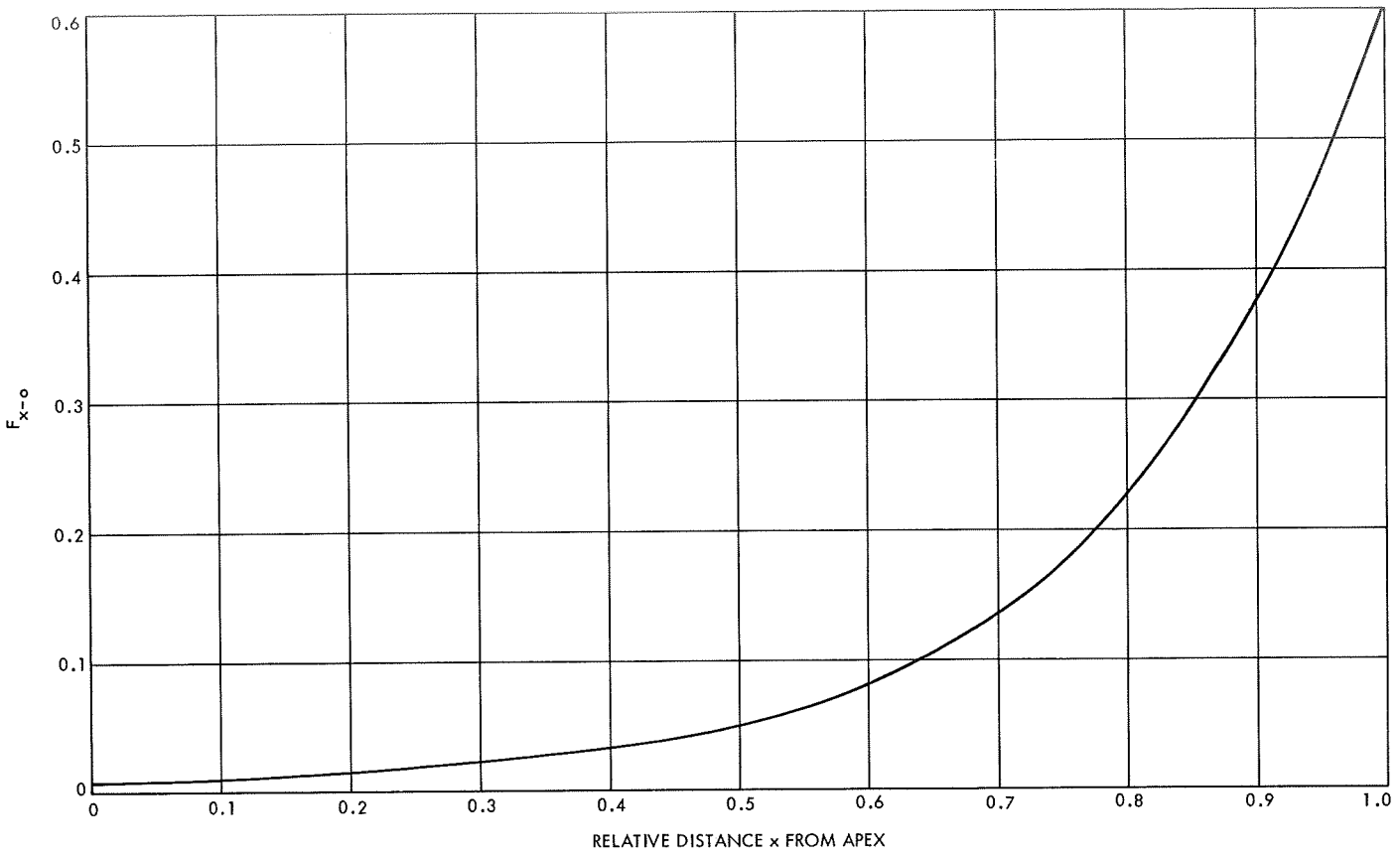

Fig. 11. F_{x-o} vs relative distance from apex

It does not follow, however, that the use of $\int K(x, y)\, dy$ in the evaluation of ϵ_a leads to results as inaccurate as might be supposed from Eq. (45). The greater accuracy of ϵ_a results from the fact that when the direct integration method is employed we use Eq. (29) directly to evaluate ϵ_a, and when we employ the series, Eq. (16), the use of Eq. (29) requires the evaluation of

$$\frac{1}{A}\int \phi_1(x)\, F_{x-o}\, da(x) \tag{46}$$

Equations (29) and (46) involve multiplying by $F_{x-o}\, da(x)$ and integrating. Notice that Eq. (41) requires multiplication by $da(x)$ only. F_{x-o} increases rapidly from the apex to the aperture, however, so the result in Eq. (29) is to weight the more accurate values of $\epsilon(x)$, those near the aperture, more heavily than those near the apex, and a similar effect applies to Eq. (46).

To see this effect on Eq. (46), recall Eq. (22),

$$\int_o^1 K(x, y) + F_{x-o} = 1 \tag{47}$$

We should have then

$$I_3 = \frac{1}{A}\int_x \left[\int_o^1 K(x, y)\, dy + F_{x-o}\right] F_{x-o}\, da(x) = 1 \tag{48}$$

If we perform this integration with $M = 100$ and fpp $= 12$, we obtain

$$I_3 = 1.00002696287 \tag{49}$$

One problem here is that we do not know the contribution to the error in I_3 from the integral

$$I_4 = \frac{1}{A}\int F_{x-o}^2\, da(x) \tag{50}$$

If we make the reasonable guess that the errors in I_4 are insignificant compared to the errors in I_5;

$$I_5 = \frac{1}{A}\int_x \left[\int K(x, y)\, dy\right] F_{x-o}\, da(x) \tag{51}$$

then we have the result that the error in I_5 is 0.000027 and hence the effect of this error on ϵ_a is much less than would be expected from Eq. (45).

Returning now to the representation of $\phi_1(x)$ as $1-F_{x-o}$; so far this method is equivalent to Peavy's evaluation (Ref. 11) of the first iterative integral. However, let us extend it further. Recall

$$\phi_2(x) = \int \phi_1(y)\, K(x,y)\, dy \tag{52}$$

$$= \int (1 - F_{y-o})\, K(x,y)\, dy \tag{53}$$

$$= \int K(x,y) - \int F_{y-o}\, K(x,y)\, dy \tag{54}$$

$$= 1 - F_{x-o} - \int F_{y-o}\, K(x,y)\, dy \tag{55}$$

Similarly, if we let

$$\theta_1(x) = \int F_{y-o}\, K(x,y)\, dy \tag{56}$$

and

$$\theta_n(x) = \int \theta_{n-1}(y)\, K(x,y)\, dy \tag{57}$$

then we have

$$\phi_2(x) = \phi_1(x) - \theta_1(x) \tag{58}$$

$$\phi_3(x) = \phi_2(x) - \theta_2(x) \tag{59}$$

and in general

$$\phi_n(x) = \phi_{n-1}(x) - \theta_{n-1}(x) \tag{60}$$

Using these equations to evaluate the ϕ_i terms, we get some increase in the error in each ϕ_n due to the propagation into $\phi_n(x)$ of the error in previous ϕ_i's, but the error in $\theta_n(x)$ is less than produced by performing the integrations

$$\epsilon_n(x) = \epsilon + \rho \int \epsilon_{n-1}(x)\, K(x,y)\, dy \tag{61}$$

or

$$\phi_n(x) = \int \phi_{n-1}(y)\, K(x,y)\, dy \tag{62}$$

The error grows larger in those integrations because $\phi_{n-1}(x)$ and $\epsilon_{n-1}(x)$ are both large near the apex and smaller near the aperture, and this causes an effective multiplication of the largest errors in $K(x,y)$ and of those occurring because of finite interval size. By contrast, because of the behavior of F_{x-o} previously pointed out, the integration for the evaluation of the θ_i terms tends to minimize the errors arising from chopping and integration errors near the apex.

Using Eqs. 56–60, $\epsilon(x)$ was recalculated for the cone again using $M = 100$ and fpp = 12. The results are shown in Table 6. Not only are all of the values of $\epsilon(x)$ less than 1, but, except for the second value, they decrease monotonically, a feature missing in Table 5. The resulting apparent emissivity for the cavity from these values of $\epsilon(x)$ is

$$\epsilon_a = 0.98201494 \tag{63}$$

We still have agreement to four decimal places with the previous values, and this increases our confidence in this result.

Next, we wished to check the result of decreasing the interval size near the apex. One way to do this is to use an interval that is small near the apex and increases gradually in size away from the apex. This is the best method and has been used successfully by J. A. Plamondon and W. Bunton of the Jet Propulsion Laboratory. However, the method used here was to make all of the intervals one-half of the previous size. This was done by increasing M to 200. The resulting value was

$$\epsilon_a = 0.98199332 \tag{64}$$

This result and the preceding values all agree within four parts per 100,000. We can explore the implications of this a little further using Richardson's extrapolation formula for Simpson's rule (Ref. 20). According to this formula, if I_M is the result of integration using Simpson's rule with M intervals and I_{2M} is the result using $2M$ intervals, the extrapolated "true" value of I is

$$I = I_{2M} + \frac{1}{15}(I_{2M} - I_M) \tag{65}$$

This formula is not exactly applicable to our case because not all of the evaluations were made using Simpson's rule, but in any case I can only be estimated so Eq. (65) will furnish an acceptable estimate. Also, we will apply Eq. (65) to ϵ_a rather than to individual values of $\epsilon(x)$.

Table 6. Emissivity of cone (from series)
$M = 100$, fpp $= 12$, $\epsilon = 0.95$

Station No.	$\epsilon(x)$	Station No.	$\epsilon(x)$
1	0.99999969	52	0.99704439
2	0.99950498	53	0.99690493
3	0.99952651	54	0.99675778
4	0.99951039	55	0.99660251
5	0.99949935	56	0.99643862
6	0.99948284	57	0.99626562
7	0.99946753	58	0.99608298
8	0.99945046	59	0.99589016
9	0.99943323	60	0.99568654
10	0.99941495	61	0.99547155
11	0.99939610	62	0.99524452
12	0.99937632	63	0.99500479
13	0.99935581	64	0.99475166
14	0.99933434	65	0.99448442
15	0.99931201	66	0.99420228
16	0.99928867	67	0.99390450
17	0.99926435	68	0.99359025
18	0.99923893	69	0.99325873
19	0.99921242	70	0.99290906
20	0.99918470	71	0.99254041
21	0.99915575	72	0.99215189
22	0.99912547	73	0.99174263
23	0.99909383	74	0.99131173
24	0.99906073	75	0.99085834
25	0.99902610	76	0.99038156
26	0.99898985	77	0.98988058
27	0.99895191	78	0.98935453
28	0.99891216	79	0.98880266
29	0.99887053	80	0.98822420
30	0.99882689	81	0.98761848
31	0.99878115	82	0.98698486
32	0.99871338	83	0.98632279
33	0.99868287	84	0.98563179
34	0.99863007	85	0.98491150
35	0.99857464	86	0.98416161
36	0.99851645	87	0.98338197
37	0.99845533	88	0.98257251
38	0.99839111	89	0.98173331
39	0.99832362	90	0.98086455
40	0.99825266	91	0.97996655
41	0.99817805	92	0.97903975
42	0.99809955	93	0.97808473
43	0.99801696	94	0.97710219
44	0.99793002	95	0.97609297
45	0.99783850	96	0.97505797
46	0.99774210	97	0.97399827
47	0.99764057	98	0.97291499
48	0.99753357	99	0.97180938
49	0.99742081	100	0.97068275
50	0.99730194	101	0.96953510
51	0.99717659		

Then if we use $I_M = 0.98201494$ and $I_{2M} = 0.98199332$, we obtain

$$\epsilon_a = I = 0.98199188 \tag{66}$$

Comparing this estimate to all previous values still shows agreement within four parts per 100,000.

Finally, we increased the precision from fpp $= 12$ to fpp $= 24$. The approach was roughly that suggested in Ref. 21: double the precision and compare the results. The leading digits that do not change are probably accurate.

The result of this calculation was

$$\epsilon_a = 0.98201449 \tag{67}$$

All of the results obtained agree within four parts per 100,000, and we conclude therefore that the correct value is

$$\epsilon_a = 0.9820 \tag{68}$$

and furthermore that four significant figures can be retained except in those cases where ρ^5 is large enough to limit the accuracy to three significant figures. This limit occurs for $\epsilon \leq 0.86$, so Table 4, for example, shows values of ϵ_a to three decimal places for $\epsilon \leq 0.86$.

It should be emphasized that, unlike the treatment of truncation errors, the preceding treatment of integration and chopping errors is not rigorous, so only an estimate of the accuracy is obtained, not a rigorous bound on the errors.

Since we have now an estimate of the accuracy of the calculations for the cone, we can by analogy assume that the calculations for the other cavities Ia and Ie are of comparable accuracy. The integration errors should be essentially the same for these cavities. Because of the complexities of the view factor formulas for cavities Ia and Ie, greater chopping errors may occur. However, the results with 12 and 24 digit precision for the cone differed by only five digits in the seventh place, so the assumption of four place accuracy is considered conservative, even for cavities Ia and Ie. There is one additional point that should be mentioned concerning the emissivity at the apex, $\epsilon(0)$. Peavy (Ref. 11) has obtained the liimting value of $\epsilon(0)$ using L'Hôpital's rule, and this value was used in computing the $\epsilon(x)$ shown in Table 5. However, it was not used for succeeding calculations for two reasons:

(1) The value of $\epsilon(0)$ does not effect the value of $\epsilon(y)$ for $y > 0$. We can see this by substituting $x \neq 0$, $y = 0$ into $K(x, y)$ for the cone. ($K(x, y)$ is given in the appendix.)

(2) $\epsilon(0)$ has no effect on ϵ_a, when Eq. (9) is used, since $F_{x-o}\, da(x) = 0$ for $x = 0$. (F_{x-o} is also given in the appendix.)

C. Accuracy of Approximate Calculations

By direct comparison of the values of ϵ_a in Tables 3 and 4 with the raw computer results of the approximate determination of ϵ_a discussed in Section II, it was determined that the approximate values were accurate to three decimal places for cavities Ia, Ie and II. It was assumed that the accuracy for the other cavities was the same, so three places were retained in Table 2 throughout.

V. Non-Isothermal Cavities

A. Temperature Calculations

It was considered desirable after the calculations described in the previous sections were performed to determine the departure from isothermality in the cavities and the effects of this non-isothermality on the apparent emissivity ϵ_a. The best way to do this would have been to solve a heat transfer equation for the entire cavity, taking account of all conduction, radiation, and convection. This would be extremely difficult to do. However, it was possible to carry out a perturbation method developed by J. M. Kendall, Sr. of the Jet Propulsion Laboratory to find an approximate solution.

The method starts with the usual assumptions that the cavity is:

(1) Isothermal.

(2) Gray.

(3) Uniform.

(4) Lambertian.

Under these conditions we compute $\epsilon(x)$ and ϵ_a as described in Section III. Now the total heat flux out the aperture is

$$Q = \epsilon_a \sigma T^4 A \tag{69}$$

The nominal operating condition for the cavity is $Q = 0.1$ W. Substitution in Eq. (69) allows us to evaluate T. Then we calculate the net heat flux $q(x)$ per unit area for each zone, using the formula

$$q(x) = \frac{\sigma T^4 \epsilon [1 - \epsilon(x)]}{1 - \epsilon} \tag{70}$$

(See Ref. 10 for derivation of this equation.) Multiplying Eq. (70) by $da(x)$, we have the net heat flux from each area zone $da(x)$.

We supply heat to the cavity by means of coils that apply heat uniformly to the surface over which they are wound. For the cone, this is the entire surface and for cavity Ie it is the center section. At equilibrium, this heat supplied must equal 0.1 W, in the absence of other radiative, conductive, or convective effects.

Now we perform the perturbation. We assume that conduction in the cavity shell causes an equilibrium temperature distribution to be established. Consider, for example, the portion of a conical cavity from the apex to a point described by a slant height x. See Fig. 12, where for simplicity the coordinates are the same as in Fig. 1. The net heat flux from this portion of the cone due to radiation is

$$\int_o^x q(x)\, da(x)$$

The heat supplied by the coils is

$$\int_o^x H\, da(x)$$

where H is the heat supplied per unit area. At equilibrium the heat entering the segment must equal the heat leaving it, so that the conductive flow, dQ/dt, must be given by

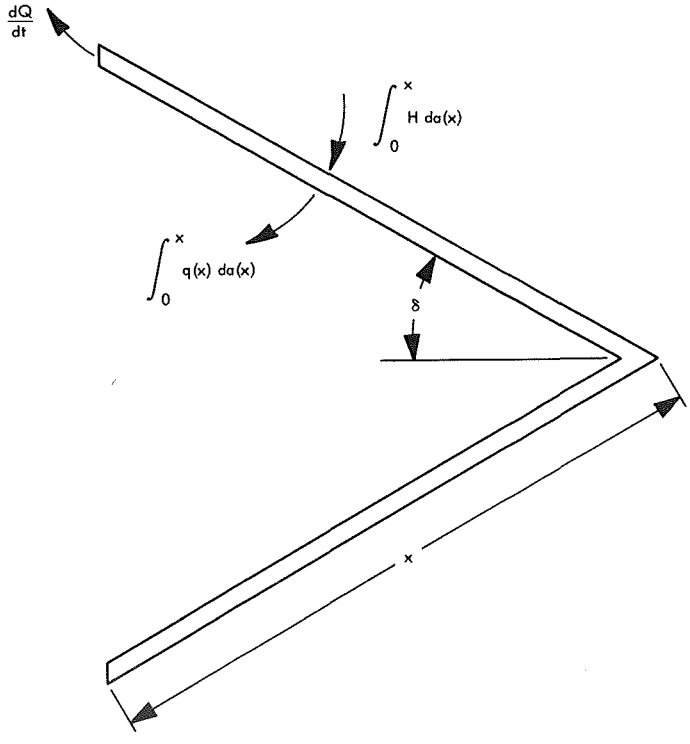

Fig. 12. Cavity heat transfer

$$\frac{dQ}{dt} = \int_o^x H\, da\,(x) - \int_o^x q\,(x)\, da\,(x) \qquad (71)$$

Now to find the temperature distribution we must solve the heat conduction equation for the cavity shell. Since only approximate answers were desired and the perturbation method is approximate in any case, it was decided to use the heat conduction equation in the form applying to linear flow,

$$\frac{dQ}{dt} = -KA\frac{dT}{dx} \qquad (72)$$

where K is the thermal conductivity of the cavity material and A is now the area of the cavity shell perpendicular to the direction of flow. For the cone of Fig. 12, for example, $A = 2\pi x d \sin\delta$.

Equation (72) was integrated numerically for the cavities previously studied, Ie (three-section cavity) and II (cone). The material of the cavity was taken to be silver, with $K = 4.18$ W per second cm deg C. For cavity Ie, the thickness d used was 0.010 in. = 0.0254 cm, and heat was assumed to be applied only to the center section. For cavity II, $d = 0.005$ in. = 0.0127 cm. The results are plotted in Figs. 13 and 14 for cavity Ie and II respectively. The abscissa y is the distance from the aperture. The ordinate is $\Delta T = T - T_o$ where T is the temperature at y and T_o is the temperature at the aperture.

B. Emissivity Calculations

The equation to be solved when the cavity is not isothermal is

$$\mathrm{B}\,(x) = \epsilon\sigma T^4\,(x) + \rho\int \mathrm{B}\,(x)\, K\,(x, y)\, dy \qquad (73)$$

where $\mathrm{B}\,(x)$ is the exitance at x. See Ref. 14, for a generalized form of this equation, where slightly different nomenclature is used.

To compare the solution of this equation with previous results, it is reasonable to define an emissivity $\epsilon\,(x)$;

$$\epsilon\,(x) = \frac{\mathrm{B}\,(x)}{\sigma T_1^4} \qquad (74)$$

Here T_1 is some average temperature in the cavity. Making the substitution Eq. (74), Eq. (73) takes the form

$$\epsilon\,(x) = \frac{\epsilon\sigma T^4\,(x)}{T_1^4} + \rho\int \epsilon\,(x)\, K\,(x, y)\, dy \qquad (75)$$

This equation can be solved by direct iteration. However, there are two problems. The results of the temperature calculations give only ΔT, the temperature referred to the temperature at the aperture. Also it is not clear which T_1 should be used.

For the cone, the following steps were used:

(1) Determine T_1 from

$$0.1 = \sigma T_1^4 A \qquad (76)$$

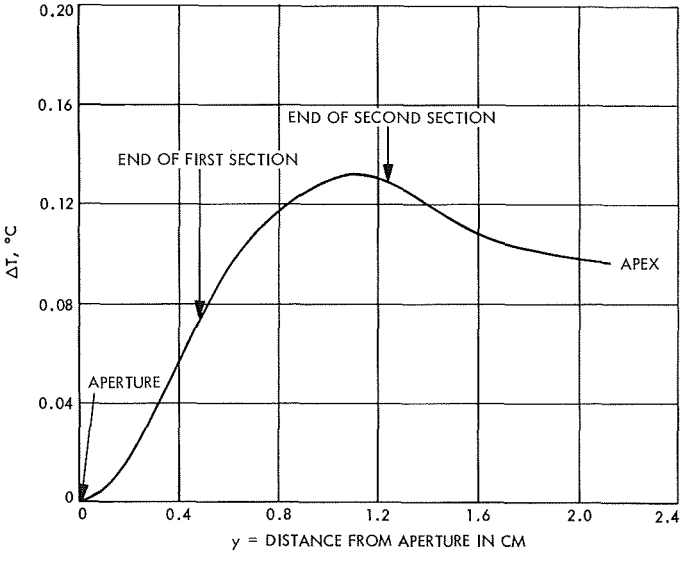

Fig. 13. Relative temperature in three-section cavity

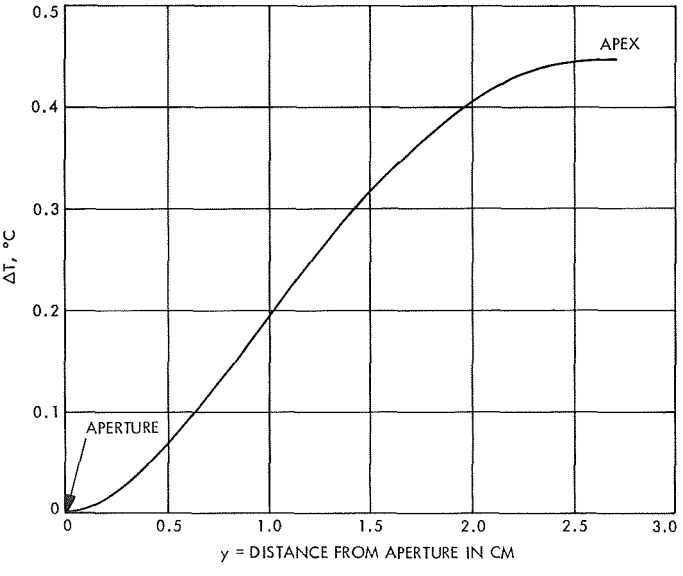

Fig. 14. Relative temperature in cone

where A in this case is again the aperture area. The result was $T_1 = 364.8°K$. Of course other T_1 values could have been used, but this was thought satisfactory for a trial.

(2) Determine ΔT_{av} from

$$\Delta T_{av} = \frac{1}{S}\int_S \Delta T(x)\, da \tag{77}$$

where S is the surface area of the cone and da is an element of area on the cone. Thus, ΔT_{av} represents the average temperature over the surface of the cone. ΔT is as given in Fig. 11.

(3) Let

$$T(x) = \Delta T - \Delta T_{av} + T_1 \tag{78}$$

The result of using this T_1, ΔT_{av}, and $T(x)$ was

$$\epsilon_a = 0.9809 \tag{79}$$

which should be compared with the isothermal value

$$\epsilon_a = 0.9820 \tag{80}$$

It can be seen that the non-isothermality causes a small but significant change, 0.0011, in ϵ_a.

The method was applied to cavity Ie where now we used

$$\Delta T_{av} = \frac{1}{(XL_2 - XL_1)}\int_{XL_1}^{XL_2} \Delta T(x)\, dx \tag{81}$$

ΔT_{av} in this case represents the average temperature over the center section of the cavity, which is the only section where heat is applied and temperature is sensed. The value $T_1 = 364.8°K$ was still used. The result was

$$\epsilon_a = 0.99226326 \tag{82}$$

which rounds off to

$$\epsilon_a = 0.9923 \tag{83}$$

Recall that the isothermal emissivity was

$$\epsilon_a = 0.9909 \tag{84}$$

Again there is a small but significant change.

To see the effect of a change in T_1, ϵ_a was recomputed for cavity Ie, using

$$0.1 = 0.9909\, \sigma T^4 A \tag{85}$$

which gave $T_1 = 363.7°K$ and

$$\epsilon_a = 0.99226915 \tag{86}$$

which rounds off to

$$\epsilon_a = 0.9923 \tag{87}$$

That is, this small temperature change produces no change in ϵ_a within the accuracy of the calculations.

VI. Non-Gray Cavities

In this section, the assumption is dropped that the cavity is gray. We still assume that it is:

(1) Isothermal.

(2) Uniform.

(3) Lambertian.

If ϵ is a function of wavelength λ,

$$\epsilon = \epsilon(\lambda) \tag{88}$$

then the following equations replace Eqs. (3) and (25)

$$\epsilon(\lambda, x) = \epsilon(\lambda) + \rho(\lambda)\int \epsilon(\lambda, x)\, K(x, y)\, dy \tag{89}$$

$$\epsilon_a(\lambda) = \frac{1}{A}\int \epsilon(\lambda, x)\, F_{x-o}\, da(x) \tag{90}$$

These equations are solved in exactly the same way as before, but they must now be solved for each λ in the range of interest.

Once we have obtained the set of $\epsilon_a(\lambda)$, we can define an apparent emissivity for the cavity for the wavelength interval (λ_1, λ_2) by the equation

$$\epsilon_a = \frac{\int_{\lambda_1}^{\lambda_2} \epsilon_a(\lambda)\, e_{b\lambda}\, d\lambda}{\int_{\lambda_1}^{\lambda_2} e_{b\lambda}\, d\lambda} \tag{91}$$

In this equation $e_{b\lambda}$ is the Planck black-body function (Ref. 14):

$$e_{b\lambda} = \frac{C_1}{n^2\lambda^5\left(\exp\frac{C_2}{n\lambda T} - 1\right)} \qquad (92)$$

where the constants in this equation are as follows, in cgs units:

$C_1 = 3.74 \times 10^{-5}$ erg cm^2/s

$C_2 = 1.4387$ cm°K

n = index of refraction of surrounding medium

T = absolute temperature in °K

Equation (91) gives ϵ_a as the ratio of the power emitted by the cavity to the power emitted by a black body of area equal to the aperture area of the cavity. Notice that ϵ_a depends not only on the wavelength interval under consideration but also on the temperature through $e_{b\lambda}$.

If $\epsilon(\lambda)$ is available, and it is desired to solve Eq. (89) and use Eq. (90) for an appropriate set of λ, Eq. (16) can be used to evaluate the large number of $\epsilon_a(\lambda)$ needed in Eq. (91), since solving Eq. (89) reduces to solving Eq. (3) at a specified set of emissivities ϵ. However, within the accuracy of the approximate solution, the values obtained by Treuenfels' method and given in Table 2 are also acceptable. These values are used here. Use is also made of values of $\epsilon(\lambda)$ for Parsons' black lacquer excerpted from data obtained in experiments at the U. S. Naval Weapons Center, Corona, California (personal communication from Dr. D. L. Stierwalt). The values used are shown graphically in Fig. 15 and are reproduced by permission of Dr. D. L. Stierwalt. The term "emittance" is used in this curve instead of the term "emissivity" used in the remainder of this report.

In Table 7, ϵ_a is presented for the cone, cavity II, for the three-section cavity, Ie, and for a flat plate, for absolute temperature T in the range 250°K to 500°K and for wavelength in the range 2–25 microns. More significant figures are retained than justified by the discussion in Section IV so that the change in ϵ_a with temperature can be studied. Also, since these temperatures differ widely from the temperature $T = 180$°C at which the $\epsilon(\lambda)$ data were obtained, some slight inaccuracy can be expected due to the change in $\epsilon(\lambda)$ with temperature. However, the significance of Table 7 is still clear: the wavelength dependence of ϵ does cause a small change in ϵ_a with temperature.

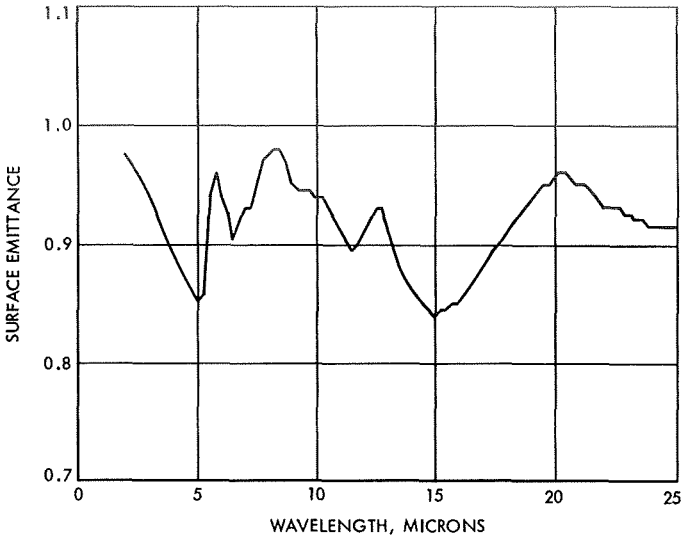

Fig. 15. Emittance vs wavelength of Parsons' black lacquer at 180°C (Excerpted from data obtained by Dr. D. L. Stierwalt of the U.S. Naval Weapons Center, Corona, California)

Table 7. Apparent emissivity ϵ_a for a range of cavity temperature, where surface emissivity ϵ has a specific wavelength dependence

T, °K	Apparent emissivity, ϵ_a		
	Cavity II	Cavity Ie	Flat plate
250	0.96765725	0.98477142	0.91269510
260	0.96793739	0.98490519	0.91341870
270	0.96821137	0.98503565	0.91412673
280	0.96847472	0.98516137	0.91480689
290	0.96872358	0.98527973	0.91544976
300	0.96895307	0.98538926	0.91604345
310	0.96916301	0.98548997	0.91658462
320	0.96935198	0.98557994	0.91707106
330	0.96951785	0.98565893	0.91750081
340	0.96966178	0.98572835	0.91787217
350	0.96978409	0.98578616	0.91818699
360	0.96988539	0.98583446	0.91844875
370	0.96996591	0.98587298	0.91865692
380	0.97002806	0.98590270	0.91881655
390	0.97007250	0.98592413	0.91893110
400	0.97010124	0.98593748	0.91900386
410	0.97011445	0.98594391	0.91903872
420	0.97011596	0.98594511	0.91904069
430	0.97010531	0.98593983	0.91901249
440	0.97008478	0.98593012	0.91895884
450	0.97005550	0.98591637	0.91888316
460	0.97001993	0.98589932	0.91878913
470	0.96997843	0.98587966	0.91868055
480	0.96993244	0.98585786	0.91856017
490	0.96988413	0.98583549	0.91843234
500	0.96983322	0.98581042	0.91830076

Appendix

View Factor Formulas

The view factors for cavity I (Fig. 2) are given below. Section No. 1 is nearest the aperture, section No. 2 is the cylindrical center section, and section No. 3 is the back cone. The aperture is designated by 0. Therefore, the view factor from the center section to the aperture is F_{20}, from the center to the back cone dF_{23}, etc. View factors between sections are differentials because they are between differentials of area. View factors from the cavity to the aperture are finite because they are from differential areas to finite areas. A full discussion of these differences is given in Ref. 14.

The direction and initial points of the running variables in each section are indicated in Fig. 2 by designation of the variables as x, y, z, but in the formulas, for consistency, only two variables are used, x and ξ. Recall that F_{ij} can be defined as the fraction of blackbody power emitted by area i that is received by area j. Then in the following formulas x always refers to the position of the area element from which power is emitted and ξ the position of the element which receives power. Thus in the formula for dF_{12}, x refers to an area element in section 1, ξ to an area element in section 2. In dF_{11}, x and ξ refer to different area elements in section 1, the x element radiating and the ξ element receiving. F_{10}, F_{20}, F_{30} all have just one variable, x, that is the position of a radiating element in sections 1, 2, and 3 respectively.

Other quantities appearing in these formulas are as follows:

$$A = \sin \delta_1$$

$$B = \cos \delta_2$$

$$A_2 = \sin \delta_2$$

$$B_2 = \cos \delta_2$$

Of the two remaining formulas given here, one is for $K(x, y)$, the kernel of the integral Eq. (3) for the cone. The variables are as shown in Fig. 1. The other is F_{x-o}, the view factor from x to the aperture for the cone. Again the variables are shown in Fig. 1. Both of these quantities could be derived from the other view factors, but are given in this form for convenience.

$$F_{10} = -\frac{1}{2xA}\left\{hB + xA^2 - \frac{[y_1(hB + xA^2) - 2R_1^2 xA_2^2]}{y_2^{1/2}}\right\}$$

where

$$y_1 = h^2 + R_1^2 + x^2A^2$$

$$y_2 = (h^2 + R_1^2 + x^2A^2)^2 - 4R_1^2 x^2A^2$$

$$h = (x - SL_0)\,B$$

$$dF_{11} = \frac{B^2}{2xA}\left\{1 - |\xi - x|\frac{[(\xi - x)^2 + 6\xi xA^2]}{[(\xi - x)^2 + 4\xi xA^2]^{3/2}}\right\} d\xi$$

$$dF_{12} = -\frac{1}{2xA}\left\{-B - \frac{(-By_1 + 2xhA^2 - 2h^2B)}{y_2^{1/2}} + \frac{[y_1(-hB + xA^2) - 2R_2^2 xA^2]\,(2y_1h)}{y_2^{3/2}}\right\} d\xi$$

where

$$y_1 = h^2 + R_2^2 + r_2^2$$

$$y_2 = (h^2 + R_2^2 + r_2^2)^2 - 4R_2^2 r_2^2$$

$$h = \xi + (SL_1 - x)\,B$$

$$r_2 = xA$$

$$dF_{13} = -\frac{1}{2xA}\left(-B_2 B - \frac{\{[2hB_2 - 2(SL_2 - \xi)A_2^2](-Bh + xA^2) - y_1 B_2 B + 4x(SL_2 - \xi)A^2 A_2^2\}}{y_2^{1/2}}\right.$$

$$\left. + \frac{[y_1(-Bh + xA^2) - 2(SL_2 - \xi)^2 xA^2 A_2^2]\{y_1[2hB_2 - 2(SL_2 - \xi)A_2^2] + 4x^2(SL_2 - \xi)A^2 A_2^2\}}{y_2^{3/2}}\right) d\xi$$

where

$$y_1 = h^2 + r_1^2 + r_2^2$$

$$y_2 = (h^2 + r_1^2 + r_2^2)^2 - 4r_1^2 r_2^2$$

$$h = (SL_1 - x)\,B + XL_2 - XL_1 + \xi B_2$$

$$r_1 = (SL_2 - \xi)\,A_2$$

$$r_2 = xA$$

$$F_{20} = -\frac{1}{2R_2}\left\{h - \frac{h(h^2 + R_1^2 + R_2^2)}{[(h^2 + R_1^2 + R_2^2)^2 - 4R_1^2 R_2^2]^{1/2}}\right\}$$

where

$$h = XL_1 + x$$

$$dF_{21} = -\frac{1}{2R_2}\left\{-B - \frac{(-By_1 - 2h^2 B + 2h\xi A^2)}{y_2^{1/2}} + \frac{2hy_1[h_1(-hB + \xi A^2) - 2\xi A^2 R_2^2]}{y_2^{3/2}}\right\} d\xi$$

where

$$y_1 = h^2 + r_1^2 + R_2^2$$

$$y_2 = (h^2 + r_1^2 + R_2^2)^2 - 4r_1^2 R_2^2$$

$$h = x + (SL_1 - \xi)\,B$$

$$r_1 = \xi A$$

$$dF_{22} = -\frac{1}{2R_2}\left\{-1 + \frac{1}{h}\left[\frac{(3h^2 + 2R_2^2)}{(h^2 + 4R_2^2)^{1/2}} - \frac{2(h^2 + 2R_2^2)^2}{(h^2 + 4R_2^2)^{3/2}}\right]\right\} d\xi$$

where

$$h = |x - \xi|$$

$$dF_{23} = -\frac{1}{2R_2}\left\{-B_2 + \frac{[B_2 y_1 + h(2hB_2 - 2r_1 A_2)]}{y_2^{1/2}} - \frac{hy_1[y_1(2B_2 h - 2r_1 A_2) + 4r_1 R_2^2 A_2]}{y_2^{3/2}}\right\} d\xi$$

where

$$y_1 = h^2 + r_1^2 + R_2^2$$

$$y_2 = (h^2 + r_1^2 + R_2^2)^2 - 4r_1^2 R_2^2$$

$$h = XL_2 - XL_1 + \xi B_2$$

$$r_1 = (SL_2 - \xi) A_2$$

$$F_{30} = -\frac{1}{2(SL_2 - \xi) A_2}\left\{hB_2 - r_2 A_2 - \frac{[(h^2 + R_1^2 + r_2^2)(hB_2 - r_2 A_2) + 2R_1^2 r_2 A_2]}{[(h^2 + R_1^2 + r_2^2)^2 - 4R_1^2 r_2^2]^{1/2}}\right\}$$

where

$$h = XL_2 + xB_2$$

$$dF_{31} = -\frac{1}{2r_2}\left(-BB_2 - \frac{\{-y_1 BB_2 + [hB_2 - (SL_2 - x) A_2^2](-2hB + 2\xi A^2) + 4A_2^2 A^2 (SL_2 - x)\xi\}}{y_2^{1/2}}\right.$$

$$\left. + \frac{\{y_1[hBB - (SL_2 - x) A_2^2] + 2A_2^2 (SL_2 - x)\xi^2 A^2\}[y_1(-2hB + 2\xi A^2) - 4\xi A^2 (SL_2 - x)^2 A_2^2]}{y_2^{3/2}}\right) d\xi$$

where

$$y_1 = h^2 + r_1^2 + r_2^2$$

$$y_2 = (h^2 + r_1^2 + r_2^2)^2 - 4r_1^2 r_2^2$$

$$h = (SL_1 - \xi) B + XL_2 - XL_1 + xB_2$$

$$r_1 = \xi A$$

$$r_2 = (SL_2 - x) A_2$$

$$dF_{32} = -\frac{1}{2(SL_2 - x) A_2}\left\{-B_2 + \frac{[B_2 y_1 + 2h(hB_2 - r_2 A_2)]}{y_2^{1/2}} - \frac{2hy_1[y_1(hB_2 - r_2 A_2) + 2r_1^2 r_2^2 A_2]}{y_2^{3/2}}\right\} d\xi$$

where

$$y_1 = h^2 + r_1^2 + r_2^2$$

$$y_2 = (h^2 + r_1^2 + r_2^2)^2 - 4r_1^2 r_2^2$$

$$h = XL_2 - XL_1 + xB_2$$

$$r_1 = R_2$$

$$r_2 = (SL_2 - x)\,A_2$$

$$dF_{33} = \frac{B_2^2}{2\,(SL_2 - x)\,A_2}\left\{1 - |x - \xi|\frac{[(\xi - x)^2 + 6\,(SL_2 - \xi)\,(SL_2 - x)\,A_2^2]}{[(\xi - x)^2 + 4\,(SL_2 - \xi)\,(SL_2 - x)\,A_2^2]^{3/2}}\right\} d\xi$$

$$K(x, y) = \frac{\cos^2 \delta}{2x \sin \delta}\left\{1 - |y - x|\frac{(y - x)^2 + 6yx \sin^2 \delta}{[(y - x)^2 + 4yx \sin^2 \delta]^{3/2}}\right\}$$

$$F_{x-o} = \frac{1}{2x \sin \delta}\left\{x - XL \cos^2 \delta - \frac{[XL^2\,(3 - 4 \sin^2 \delta)\,x - 3XL \cos^2 \delta\, x^2 + x^3 - XL^3 \cos^2 \delta]}{[(XL^2 + x^2 - 2xXL \cos^2 \delta)^2 - 4x^2\,XL^2 \sin^4 \delta]^{1/2}}\right\}$$

Nomenclature

A	area of cavity aperture, surface area of cavity, or sin δ
$B(x)$	exitance at point x in a cavity
E	truncation error in ϵ_a
$E(x)$	truncation error in $\epsilon(x)$
$e_{b\lambda}$	Planck blackbody function
F_{i-j}, F_{ij}	view factor from surface i to surface j
f	flatness, from Treuenfels' formula (formula 2)
fpp	floating point precision (number of digits carried in a computer calculation)
K	thermal conductivity
$K(x, y)$	kernel of integral equation (defined by $K(x, y)\,dy = dF_{x-y}$, where dF_{x-y} is a view factor)
M	number of integration intervals
N	number of integrations used in solving integral equation, or number of points used in integration
Q	radiant flux
T	temperature, °K
α	surface absorptivity of cavity
α_a	apparent absorptivity of cavity
ϵ	surface emissivity
ϵ_a	apparent emissivity of cavity
$\epsilon(x)$	apparent emissivity at a point x in a cavity
ρ	reflectivity of a surface
σ	Stefan-Boltzmann constant
ϕ_i	iterative function in solution of integral equation

References

1. Kendall, J. M., Sr., Haley, F., and Plamondon, J. A., "Cavity Type Absolute Total Radiation Radiometer," paper presented at the 20th Annual ISA Conference and Exhibit, Los Angeles, Calif., Oct. 4–7, 1965.

2. Kendall, J. M., Sr., and Plamondon, J. A., "An Absolute Cavity Radiometer for Measurement of Thermal Radiation," paper presented at the AIAA/IES/ASTM Space Simulation Conference, Houston, Texas, Sept. 7–9, 1966.

3. Kendall, J. M., Sr., *The JPL Standard Total-Radiation Absolute Radiometer*, Technical Report 32-1263. Jet Propulsion Laboratory, Pasadena, Calif., May 6, 1968.

4. Willson, Richard C., *Experimental and Theoretical Comparison of the JPL Activity Cavity Radiometric Scale and the International Pyrheliometric Scale*, Technical Report 32-1365. Jet Propulsion Laboratory, Pasadena, Calif., Feb. 1, 1969.

5. Kendall, J. M., Sr., *Primary Absolute Cavity Radiometer*, Technical Report 32-1396. Jet Propulsion Laboratory, Pasadena, Calif., July 15, 1969.

6. Sydnor, C. L., "Series Representation of the Solution of the Integral Equation for Emissivity of Cavities," *J. Opt. Soc. Am.*, Vol. 59, No. 10, pp. 1288–1290, Oct. 1969.

7. Planck, M. K., *The Theory of Heat Radiation.* Translated by M. Masius. Dover Publications, Inc., New York, 1959 (originally published as Waermastrahlung in 1913).

8. Treuenfels, E. W., "Emissivity of Isothermal Cavities," *J. Opt. Soc. Am.*, Vol. 53, pp. 1162–1171, Oct. 1963.

9. Vollmer, J., "Study of the Effective Thermal Emittance of Cylindrical Cavities," *J. Opt. Soc. Am.*, Vol. 47, pp. 926–932, Oct. 1957.

10. Sparrow, E. M., and Jonsson, V. K., "Radiant Emission Characteristics of Diffuse Conical Cavities," *J. Opt. Soc. Am.*, Vol. 53, pp. 816–821, July 1963.

11. Peavy, B. A., "A Note on the Numerical Evaluation of Thermal Radiation Characteristics of Diffuse Cylindrical and Conical Cavities," *J. Res. NBS, Sec. C*, Vol. 70, No. 2, pp. 139–147, April–June 1966.

12. Sparrow, E. M., and Jonsson, V. K., "Absorption and Emission Characteristics of Diffuse Spherical Enclosures," *Trans. ASME, Ser. C: J. Heat Transfer*, Vol. 84, pp. 188–189, 1962.

13. Sparrow, E. M., "Radiant Absorption Characteristics of Concave Cylindrical Surfaces," *Trans. ASME, Ser. C: J. Heat Transfer*, Vol. 84, pp. 283–293, 1962.

14. Sparrow, E. M., and Cass, R. D., *Radiation Heat Transfer.* Brooks/Cole Publishing Company, Belmont, Calif., 1966.

15. Lovitt, W. V., *Linear Integral Equations*, First Edition. Dover Publications, Inc., New York, 1950.

References (contd)

16. Tricomi, F. G., *Integral Equations.* Interscience Publishers (John Wiley and Sons, Inc.), New York, 1957.

17. Jones, R. C., "Immersed Radiation Detectors," *J. Appl. Opt.*, Vol. 1, pp. 607–613, 1962.

18. Nicodemus, F. E., "Radiance," *Am. J. Phys.*, Vol. 31, pp. 368–377, 1963.

20. Noble, B., *Numerical Methods: Volume II.* Oliver and Boyd, London, 1964 (Interscience Pub., Inc., New York).

21. Prager, W., *Introduction to Basic FORTRAN Programming and Numerical Methods.* Blaisdell Publishing Company, New York, 1965.

NASA — JPL — Coml., L.A., Calif.